


Exponential space-dependent heat generation on Powell–Eyring hybrid nanofluid under nonlinear thermal radiation

K Gangadhar¹ , M Prameela² and A J Chamkha^{3*}

¹Department of Mathematics, Acharya Nagarjuna University, Guntur, Andhra Pradesh 522510, India

²Department of Mathematics, Prasad V. Potluri Siddharth Institute of Technology, Kanuru, Vijayawada, Andhra Pradesh 520007, India

³Faculty of Engineering, Kuwait College of Science and Technology, 35004 Doha District, Kuwait

Received: 20 September 2022 / Accepted: 29 December 2022

Abstract: Hybrid nanofluids were popularized by heat transfer fluids into higher surface strength, dispersion and diffusion prospects related into traditional nanofluid. The novel characteristics of a single-phase hybrid nanofluid profile coincidence in studying nanoparticles mass including base fluid mass to produce solid equivalent density and addition to solid equivalent specific heat about constant pressure. On this work, flow and volumetric entropy generation and convective heat transport on Powell–Eyring hybrid nanofluid have been consider. Hybrid nanofluids attend the space through the systematic horizontal porous stretching surface. Impact on exponential space-dependent heat generation and nonlinear thermal radiation was more combined on the specified sketch. Mathematical equations about conservation of energy, mass, entropy and momentum are interpreted below acceptance on boundary layer flow of Powell–Eyring hybrid nanofluid. Comparison results were collected as conversion away from governing partial differential equations into ordinary differential equations, applying correlation variables. Finite element method was an external for finding the relative results of decreased ordinary differential equations. Numerical computing was achieved about zinc oxide–gold water (ZnO–Au/H₂O) hybrid nanofluid and conventional gold water (Au–H₂O) nanofluid. The notable allegation indicated to the hybrid Powell–Eyring nanofluid was best thermal conductor although related into a conventional nanofluid and pure water. Every rising on Reynolds number and Brinkman number developed into total entropy for that structure.

Keywords: Powell–Eyring fluid; Exponential space-dependent heat source; Hybrid nanofluid; Entropy generation; FEM

1. Introduction

In modern years, non-Newtonian fluids due to the appreciable act on industrial and engineering applications had admiring the consideration the high number of investigators. Those contain Eyring–Powell fluid, power law fluid, Prandtl fluid, Reiner–Philippoff fluid, Carreau fluid, Prandtl–Eyring fluid, Casson fluid and micropolar fluid. Fluids, for example, could be used on that refinement for chemical purposes; for example, a number of researchers were investigating non-Newtonian fluids on that method. Powell and Eyring [1] had popularized fluid figure known Eyring–Powell fluid. Timol and Patel [2] advanced to Eyring–Powell models extra effective and important by related toward the power law model, although that is fairly

convoluted on nature. Concurrently, solicitude is dispute to their fluid’s dynamic presence that was detained for the come from the fluids kinetic theory large to it was realistic interpretation. Every fluid imitation as Eyring–Powell was utilized from construction on substantial flows. Aziz et al. [3] used Keller box finite various scheme to analyze by convective heat transfer and entropy generation on Powell–Eyring nanofluid flow through the inflexible horizontal penetrable stretching surface. They concluded that the rate of heat transfer on that boundary was highest as lowest value on the shape factor parameter. Vafai et al. [4] analyzed numerically the mass and heat transfer characteristics below an impact on magnetic dipole through the stretching sheet. The entropy generation on bio-convective flow of Powell–Eyring nanofluid through porous stretched surface into cylinder was studied by Xia et al. [5]. Ibrahim [6] used semi-analytical method to analyze the concentration

*Corresponding author, E-mail: a.chamkha@kcst.edu.kw

reliant-viscosity about the peristaltic flow by non-Newtonian fluid on the convergent-divergent channel.

Nanofluids mention for the diminish suspensions on ultrafine particles on base fluids. Like as liquids had desirable thermophysical properties mention to pure working fluids. Every formation on copper, carbon and alternative greater thermal conductivity material nanoparticles into ethylene glycol, water and oils had is entrenched by the efficient direction into raise heat transfer possibility to those liquids. The remarkable thermal achievement on nanofluids necessitates that all be used on system as a result of the ever-growing objections to heat discharge on cooling functions. In 1995, that nanofluid's word is invented as Choi and Eastman [7]. Every nanofluids were constructive into raise diminish drag coefficients and/or thermal properties about function grazing to electronics cooling for microfluidics. The pendulous nanoparticles could importantly enhance by transport properties on base fluids, and that ensuing nanofluids show appealing properties like that high boiling heat transfer coefficient and high thermal conductivity [8]. Gangadhar et al. [9] considered that boundary layer flow of non-Newtonian nanofluid along an external uniform magnetic field. Lee et al. [10] carried out time-dependent and the energy density rheological performance on carbon nanotube nanofluids of sonication.

The double or different hybridizations on higher thermal conductivity nanoparticles to the broadcast with the base fluid ways of heat transfer fluid (hybrid nanofluid) that had the applicable properties whatever important on the plethora of functions specifically on the area of electronic industries, biomedical, automobile and engineering (Sarkar et al. [11], Babu et al. [12]). To this, hybrid nanofluid present had turn into primary applicable case between the investigators to well accept the mechanism behind like fluid. Mabood et al. [13] numerically considered the boundary layer investigation on two-dimensional unsteady hybrid nanofluid flow through the slandering/flat stretching surface. They found that skin friction dismiss due to nanoparticle volume fraction. Selimefendigil and Oztop [14] studied the estimate on the PCM filled three-dimensional vertical cylinder below the associate impact on surface existence and corrugation of double nanoparticles on the heat transfer fluid. Abbas et al. [15] presented theoretical analysis for the hybrid nanofluid flow previous the exponentially curved surface with the penetrable medium. Every dynamics of colloidal mixture to water into different nanoparticles as various zone of partial slip is considered as Cao et al. [16]. Zhai et al. [17] discuss detailed results for porous media, heat transfer and flow characteristics of $\text{Al}_2\text{O}_3\text{-TiO}_2/\text{water}$ nanofluids on the microchannel.

The entropy generation study was the significant tool about efficient development to the thermal systems. The complete entropy generation was entire as the inclusion on

nanoparticles along the base fluid, hence that heat transfer benefit into the entire entropy generation rate reduces. The impact on entropy generation by nanofluids on porous cavities had been consider broadly due to it is functions on industry. Avellaneda et al. [18] performed the direct numerical simulation of flow component in entropy generation rate to enforced convective turbulent channel flow on the thermo-dependent fluid. Devi et al. [19] explored the review for generation on entropy and mass and heat transfer improvement working porous media and nanoparticle. Gowtham et al. [20] recycled finite volume method for modeled entropy optimization and the heat transfer inside the curved courtyard employing local heater by the under boundary. Marzougui et al. [21] studied the entropy generation on mixed convection on the lid-driven porous close to filled over the nanoliquid on the consideration to uniform magnetic field. Their study explored to the total entropy reduced with the nanoparticle volume fraction. Sarbazi and Hormozi [22] performed the analysis of thermal-hydrodynamic features into silicon water/oxide nanofluid laminar flow on the heat sink miniature channel among various fin cross sections. Mehta et al. [23] inspected the basic role on the entropy generation components about laminar flow of water over the ribbed-curved channel.

This method of generating heat energy into the fluid flow structure was called by constitutional heat generation. Every internal heat generation gives the aggressive design into energy equation on fluid flow issues. The aggressive heat source had giant functions on engineering and industries fields. Sadiq et al. [24] analyzed numerically by stagnation point flow on micropolar fluid about unsteady flow. Their results indicated that temperature distribution upsurges on increasing Eckert number. Nagaraja and Gireesha [25] discussed the aggressive space-reliant heat source of MHD Casson fluid flow through the wavy stretching sheet including mass and heat flux boundary condition and chemical reactions. Berrehal et al. [26] examined the impact on heat source/sink by the motion of nanofluid flowing across the stretching sheet on the existence of entropy generation. Quan et al. [27] reported that effect on MHD flow by micropolar fluid over exponentially wavy surface. Gangadhar et al. [28] investigated the magnetized couple stress fluid through a porous stretching cylinder along non-uniform heat source. Also, recently, the heat transfer within fluid flow having different surfaces was considered by many investigators [29–49].

About the investigation of the upper-presented literature, irreversibility study on Powell Eyring $\text{ZnO-Au/H}_2\text{O}$ hybrid nanofluid flow in the combined impacts of nonlinear thermal radiation and aggressive space-dependent heat source in the presence of convective heat flux boundary condition have not earlier considered. Hence, it was the

primary goal of the present analysis. Four key problems identical into the heat transfer condition of Powell–Eyring hybrid nanofluid (here, ZnO–Au/water) had been forward about the first time. Where, Au–ZnO/water nanofluid was unfamiliar by the illustration to the synthetic hybrid nanofluid being synthetic model by that form of hybrid nanofluid had be described on the article, thus its thermo-physical details were applicable. Furthermore, gold nanoparticles are called as anti-bacterial agents.

1. Which occur to convective heat transfer of the existence on hybrid nanofluids? Did the heat transfer improve when the enhancement on Biot number or depreciate by cause of the improvement about heat absorption?
2. Do several thermal improvements into using water-based Au–ZnO hybrid nanofluid related by the common water-based nanofluid and pure water?
3. Did developing the volume fraction about Au nanoparticles along the base fluid constantly improve heat transfer?
4. What happens of drag skin friction coefficient in the presence of Powell–Eyring hybrid nanofluid? Did rising into volume fraction by Au nanoparticles always deteriorate that density of the momentum boundary layer?

Beneficial for interpretation the upper component key computations, they continue into the after field of propose the physical sketch about the heat transfer and the flow on the Powell–Eyring hybrid nanofluid through the infinite penetrable flat surface. That analysis was very innovative and advanced situated the new direction into the better of our ability.

2. Mathematical model and governing equations

Examine boundary layer flow of incompressible, laminar, stable, unsteady, optically thick hybrid nanofluid through the infinite porous plate. The Non-Newtonian Powell–Eyring mathematical figure was affected about the hybrid nanofluid. That Cartesian dimensional coordinates were affected to x_1 -axes with the penetrable surface, and y_1 -axes were common into that. The surface demonstrates the plane $y_1 = 0$. This flow was arising when the non-uniform stretching by the plate. The oblique surface on the plate was heated when the convection into the uniform hot fluid, and the temperature outside the plate was fixed. Those radiations could only travel the little range into optically thick nanofluid; accordingly, Rosseland resemblance was given with account about radiative heat transfer. That was the uniform circulation of nanoparticles to the base fluid, and the capacity of the nanoparticles was uniform.

Certainly, the thermal equilibrium was assisted into nanoparticles and base fluid and that was not error among it. The nanofluid figure suggested as Das and Tiwari [37] was study to that work. The geometry of the sketch is displayed in Fig. 1.

The nanofluid was assembled as computing gold (Au) nanoparticle on pure water base fluid to that contact volume friction is φ . Later gold (Au) and zinc oxide (ZnO) nanoparticles to the contact volume frictions of φ_1 and φ_2 were circulated on the nanofluid for assembled hybrid nanofluid. That nanoparticle volume concentration coefficient by hybrid nanofluid was defend by $\varphi_{\text{hnf}} = \varphi_1 + \varphi_2$. The constitutive equation on Powell–Eyring fluid is copied against the theory on liquids and nothing into the observational contact by the power-law figure. Powell–Eyring fluid figure decreases into Newtonian flow performance for below and above shear rates. On correlation, power law fluid figure illustrates the infinite active viscosity to below shear rate and hence, confines its distance on relevance. The Cauchy stress tensor about Powell–Eyring fluid was taken by (seen about example, [1])

$$\tau_{ij} = \mu_{\text{hnf}} \left[\frac{\partial(u_1)_i}{\partial(x_1)_j} \right] + \frac{1}{\beta} \sinh^{-1} \left[\frac{1}{\hat{\zeta}} \frac{\partial(u_1)_i}{\partial(x_1)_j} \right]. \quad (1)$$

Here, μ_{hnf} was the hybrid dynamic viscosity on hybrid Powell–Eyring nanofluid, and $\hat{\beta}, \hat{\zeta}$ is material constants. The temperature and stretching velocity about penetrable surface was

$$U_w(x_1, t_1) = \frac{cx_1}{1 - \tilde{\omega}t_1}, \quad T_w(x_1, t_1) = T_\infty + \frac{cx_1}{1 - \tilde{\omega}t_1}, \quad (2)$$

where $\tilde{\omega}$ as the unsteadiness parameter into $\tilde{\omega} = 0$ corresponds to steady linear stretching/flow. t_1 as the time and c as a positive constant. T_∞ as the ambient temperature. $\frac{1}{1 - \tilde{\omega}t_1}$ as the effective stretching rate.

This governing equations about conservation of energy, momentum and mass below the boundary layer acceptance

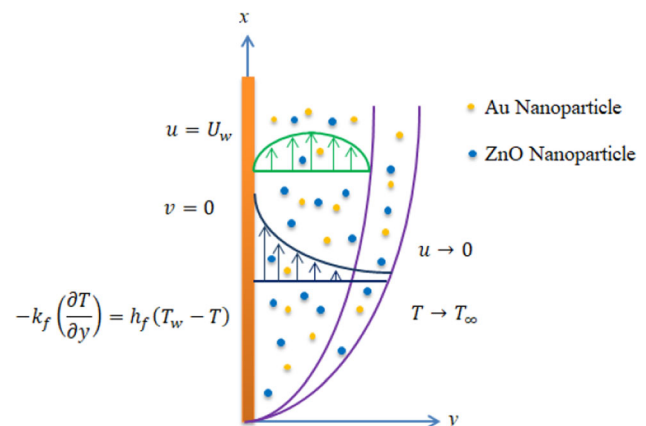


Fig. 1 Physical model on aspect to coordinates structure

forward into applicable boundary conditions by hybrid Powell–Eyring nanofluid could be drafted by (for specifics see, [3, 38])

$$\frac{\partial u_1}{\partial x_1} + \frac{\partial v_1}{\partial y_1} = 0, \quad (3)$$

$$\frac{\partial u_1}{\partial t_1} + u_1 \frac{\partial u_1}{\partial x_1} + v_1 \frac{\partial u_1}{\partial y_1} = \left[v_{\text{hnf}} + \frac{1}{\rho_{\text{hnf}} \hat{\beta} \hat{\zeta}} \right] \frac{\partial^2 u_1}{\partial y_1^2} - \frac{1}{2 \hat{\beta} \hat{\zeta}^3 \rho_{\text{hnf}}} \left[\frac{\partial u_1}{\partial y_1} \right]^2 \frac{\partial^2 u_1}{\partial y_1^2}, \quad (4)$$

$$\begin{aligned} \frac{\partial T_1}{\partial t_1} + u_1 \frac{\partial T_1}{\partial x_1} + v_1 \frac{\partial T_1}{\partial y_1} &= \frac{k_{\text{hnf}}}{(\rho C_p)_{\text{hnf}}} \frac{\partial^2 T_1}{\partial y_1^2} - \frac{1}{(\rho C_p)_{\text{hnf}}} \left[\frac{\partial q_r}{\partial y_1} \right] \\ &+ \frac{\mu_{\text{hnf}}}{(\rho C_p)_{\text{hnf}}} \left[\frac{\partial u_1}{\partial y_1} \right]^2 + \frac{Q_0}{(\rho C_p)_{\text{hnf}}} \\ &(T_1 - T_\infty) \exp\left(-\frac{c}{v_f(1 - \hat{\omega} t_1)} y_1\right) \end{aligned} \quad (5)$$

$$u_1(x_1, 0) = U_w, v_1(x_1, 0) = 0, -k_f \left[\frac{\partial T_1}{\partial y_1} \right] = h_f(T_w - T_1), \quad (6)$$

$$u_1 \rightarrow 0, T_1 \rightarrow T_\infty \text{ as } y_1 \rightarrow \infty. \quad (7)$$

where u_1 and v_1 were horizontal and vertical velocities, appropriately. $\mu_{\text{hnf}}, \rho_{\text{hnf}}, k_{\text{hnf}}, (\rho C_p)_{\text{hnf}}$ and q_r are thermal conductivity, density, thermal radiation factor of hybrid nanofluid, specific heat capacity and viscosity. k_f and h_f are heat transfer coefficient and thermal conductivity on base fluid, appropriately. Subsequent Refs. [31–36], the special similarity among thermophysical properties of base fluid and nanofluid is introduced. These relations are given in Table 1. To optically thick hybrid nanofluid, that nonlinear thermal radiation q_r could have drafted by (by specifics see [39])

$$q_r = -\frac{16\sigma_* T_1^3}{3k_s} \frac{\partial T_1}{\partial y_1}, \quad (8)$$

where, k_s as the absorption coefficient and σ_* as the Stefan Boltzmann number.

To achieve as comparison explanation into the constitutive structure by partial differential Eqs. (3)–(5) object that boundary conditions (6)–(7), consecutive Aziz et al. [3], the correlated variable ξ and stream functions Ψ and θ was affected by

$$u_1 = \frac{\partial \Psi}{\partial y_1}, v_1 = -\frac{\partial \Psi}{\partial x_1}, \quad (9)$$

$$\begin{aligned} \xi(x_1, y_1) &= \sqrt{\frac{c}{v_f(1 - \hat{\omega} t_1)}} y_1, \Psi(x_1, y_1) \\ &= \sqrt{\frac{c}{(1 - \hat{\omega} t_1)}} x_1 g(\xi), \\ \theta(\xi) &= \frac{T - T_\infty}{T_w - T_\infty}. \end{aligned} \quad (10)$$

Substituting in Eqs. (9) and (10) on governing system (3)–(7) and formulation help on relations taken as Eq. (8) gives

$$\begin{aligned} \left(\frac{1}{\varphi_a \varphi_b} + \frac{\omega}{\varphi_a} \right) g''' + g g'' - g'^2 - A \left(g' + \frac{\xi}{2} g'' \right) \\ - \frac{\omega \Delta}{\varphi_b} g'^2 g''' \\ = 0, \end{aligned} \quad (11)$$

$$\begin{aligned} \frac{1}{\varphi_c} \frac{d}{d\xi} \left\{ \left(1 + \frac{4\text{Rd}}{3\varphi_d} (1 + (\theta_w - 1)\theta)^3 \right) \theta' \right\} \\ + \text{Pr} \frac{\varphi_c}{\varphi_d} \left[g \theta' - g' \theta - A \left(\theta + \frac{\xi}{2} \theta' \right) \right. \\ \left. + \frac{Ec}{\varphi_a \varphi_c} g'^2 + \frac{Q}{\varphi_c} \theta e^{-\xi} \right] = 0, \end{aligned} \quad (12)$$

$$g(0) = 0, g'(0) = 1, \theta'(0) = -\frac{\text{Bi}}{\varphi_d} (1 - \theta(0)), \quad (13)$$

$$g'(\xi) \rightarrow 0, \theta(\xi) \rightarrow 0, \text{ as } \xi \rightarrow \infty, \quad (14)$$

with

$$\varphi_a = (1 - \varphi_1)^{2.5} (1 - \varphi_2)^{2.5}, \quad (15)$$

$$\varphi_b = (1 - \varphi_2) \left\{ (1 - \varphi_1) + \varphi_1 \frac{\rho_{p1}}{\rho_f} \right\} + \varphi_2 \frac{\rho_{p2}}{\rho_f}, \quad (16)$$

Table 1 Thermophysical properties to the base fluid and the nanoparticles by 25 °C [31–36]

Thermophysical properties	Fluid phase (water) [31, 32]	Zinc oxide (ZnO) [33, 34]	Gold (Au) [35, 36]
C_p (J kg ⁻¹ K ⁻¹)	4179	495.2	129
ρ (k gm ⁻³)	997.1	5600	19,282
k (W m ⁻¹ K ⁻¹)	0.613	13	310
Particle size/nm	–	29 and 77	3–40

$$\varphi_c = (1 - \varphi_2) \left\{ (1 - \varphi_1) + \varphi_1 \frac{(\rho C_p)_{p_1}}{(\rho C_p)_f} \right\} + \varphi_2 \frac{(\rho C_p)_{p_2}}{(\rho C_p)_f}, \quad (17)$$

$$\varphi_d = \frac{\left[\frac{(k_{p_2}\varphi_2 + k_{p_1}\varphi_1)}{\varphi_1 + \varphi_2} + 2\kappa_f \right] - 2(\varphi_1 + \varphi_2) \left(\kappa_f - \frac{k_{p_2}\varphi_2 + k_{p_1}\varphi_1}{\varphi_1 + \varphi_2} \right)}{\left[\frac{(k_{p_2}\varphi_2 + k_{p_1}\varphi_1)}{\varphi_1 + \varphi_2} + 2\kappa_f \right] + (\varphi_1 + \varphi_2) \left(\kappa_f - \frac{k_{p_2}\varphi_2 + k_{p_1}\varphi_1}{\varphi_1 + \varphi_2} \right)}. \quad (18)$$

Here, $A = \frac{\hat{\omega}}{c}$ is the unsteadiness parameter, $\omega = \frac{1}{\mu_f \beta \hat{\zeta}}$ and $\Delta = \frac{U_w^3}{2c^2 \nu_f x_1}$ was the material parameters, $\text{Pr} = \frac{\nu_f}{\alpha_f}$ as the Prandtl number, $\text{Rd} = \frac{4\sigma_w T_\infty^3}{k_s \nu_f (\rho C_p)_f}$ is the thermal radiation factor, $\text{Ec} = \frac{U_w^2}{(C_p)_f (T_w - T_\infty)}$ is the Eckert number, $\text{Bi} = \frac{h_f}{k_f} \sqrt{\frac{\nu_f (1 - \hat{\omega} t_1)}{c}}$ is the Biot number, $\theta_w = \frac{T_w}{T_\infty}$ as the temperature ratio parameter and $Q = \frac{Q_0}{c(\rho C_p)_f}$ is the heat source/sink parameter. In Eqs. (15)–(18), κ_{nf} as the thermal conductivity on the nanofluid and $\rho_f, (C_p)_f$ and κ_f as effective heat capacity, density and thermal conductivity to the base fluid, appropriately. These p_1 perform the gold solid nanoparticle, and p_2 perform the zinc oxide solid nanoparticles. The other properties such as $\rho_{p_1}, \rho_{p_2}, (C_p)_{p_1}, (C_p)_{p_2}, \kappa_{p_1}$ and κ_{p_2} are the thermal conductivity, specific heat capacity and density of the gold and zinc oxide solid nanoparticles, appropriately (Table 1).

That physical quantities applicable to that work was local Nusselt number (Nu_x) and skin friction factor (C_f). Those are defined by

$$C_f = \frac{\tau_w}{\rho_f U_w^2}, \quad \text{Nu}_x = \frac{x_1 q_w}{k_f (T_w - T_\infty)}, \quad (19)$$

here τ_w and q_w taken by

$$\tau_w = \left[\left(\mu_{\text{hnf}} + \frac{1}{\hat{\beta}\hat{\zeta}} \right) \frac{\partial u_1}{\partial y_1} - \frac{1}{6\hat{\beta}\hat{\zeta}^3} \left(\frac{\partial u_1}{\partial y_1} \right)^3 \right]_{y_1=0}, \quad (20)$$

$$q_w = -\kappa_{\text{hnf}} \left(\frac{\partial T_1}{\partial y_1} \right)_{y_1=0} + (q_r)_{y_1=0}.$$

Into the advice of Eq. (9) and (10), the dimensionless pattern is

$$C_f \text{Re}_x^{\frac{1}{2}} = \left[\left(\frac{1}{(1 - \varphi_1)^{2.5} (1 - \varphi_2)^{2.5}} + \omega \right) g''(0) - \frac{\omega \Delta}{3} (g''(0))^3 \right],$$

$$\text{Nu}_x \text{Re}_x^{\frac{1}{2}} = - \left\{ \frac{\kappa_{\text{hnf}}}{\kappa_f} + \frac{4\text{Rd}}{3} (1 + (\theta_w - 1)\theta(0))^3 \right\} \theta'(0). \quad (21)$$

Here, $\text{Re}_x = \frac{x_1 U_w}{\nu_f}$ was the local Reynolds number.

3. Analysis of entropy generation and Bejan number

Every Local volumetric rate about entropy generation EG about the figure was conveyed by on Kuman et al. [40]

$$\text{EG} = \frac{\kappa_{\text{hnf}}}{T_\infty^2} \left(\left(\frac{\partial T_1}{\partial y_1} \right)^2 + \frac{16\sigma_w}{3k_s \kappa_{\text{hnf}}} T_1^3 \left(\frac{\partial T_1}{\partial y_1} \right)^2 \right) + \frac{\mu_{\text{hnf}}}{T_\infty} \left(\frac{\partial u_1}{\partial y_1} \right)^2, \quad (22)$$

here, these first term was the Local entropy generation when the heat transfer into thermal radiation and that second term was the Local entropy generation when the viscous dissipation. That non-dimensional entropy generation rate was taken as

$$\text{Ns} = \frac{\text{EG}}{E_0} = \text{Re} \varphi_d \left[1 + \frac{4\text{Rd}}{3\varphi_d} (1 + (\theta_w - 1)\theta(\xi))^3 \right] \theta'(\xi)^2 + \text{Re} \frac{\text{Br}}{\Omega} \frac{1}{\varphi_a} (g''(\xi))^2. \quad (23)$$

The definition about Bejan number to the present analysis as

$$\text{Be} = \frac{\varphi_d \left[1 + \frac{4\text{Rd}}{3\varphi_d} (1 + (\theta_w - 1)\theta(\xi))^3 \right] \theta'(\xi)^2}{\varphi_d \left[1 + \frac{4\text{Rd}}{3\varphi_d} (1 + (\theta_w - 1)\theta(\xi))^3 \right] \theta'(\xi)^2 + \frac{\text{Br}}{\Omega} \frac{1}{\varphi_a} (g''(\xi))^2}. \quad (24)$$

The irreversibility ratio is defined as

$$\Phi = \frac{\frac{\text{Br}}{\Omega} \frac{1}{\varphi_a} (g''(\xi))^2}{\varphi_d \left[1 + \frac{4\text{Rd}}{3\varphi_d} (1 + (\theta_w - 1)\theta(\xi))^3 \right] \theta'(\xi)^2}, \quad (25)$$

where $E_0 = \frac{k_f (T_w - T_\infty)^2 c}{T_\infty^2 \nu_f}$ as the characteristic entropy generation rate, $\text{Re} = \frac{U_w c^2}{\nu_f x_1}$ as the Reynolds number, $\text{Br} = \text{Pr Ec}$ as the Brinkman number and $\Omega = \frac{T_w - T_\infty}{T_\infty}$ as dimensionless temperature gradient.

4. Numerical method

This designed problems (11)–(12) were defined numerically by FEM method that was powerful technique and had being utilized on various current analysis [14, 21, 23]. The accurate method was established under:

4.1. Discretization of domain

That step contains separation body along with equivalent structure on small segments, known as ‘finite elements.’ That current form of domain was single discretized and dimensional with line segment, double nodes by segment.

4.2. Select approximation functions

On that step, they accept the model or form about the circulation to the exotic capacity into every component. In that container on line component (double nodes by component), linear shape function was utilized that was taken as

$$\Omega_j = (-1)^{j-1} \left(\frac{\xi_{j+1} - \xi}{\xi_{j+1} - \xi_j} \right), \quad j = 1, 2. \quad (26)$$

4.3. Selection of weight functions

Various forms were worked about the excerpt by weight function. On GFEM, shape functions were given by weight functions.

4.4. Construction of residuals and weak form

These weighted integral model in fragment about doubled nonlinear structure of boundary value problems (11)–(12) by typical components (ξ_b, ξ_{b+1}) is

$$\int_{\xi_{b+1}}^{\xi_b} w_i (g' - h) d\xi = 0, \quad (27)$$

$$\int_{\xi_{b+1}}^{\xi_b} w_i \left(\left(\frac{1}{\varphi_a \varphi_b} + \frac{\omega}{\varphi_a} \right) h'' + g h' - h^2 - A \left(h + \frac{\xi}{2} h' \right) - \frac{\omega \Delta}{\varphi_b} h'^2 h'' \right) d\xi = 0, \quad (28)$$

reliant variables with f, θ and h were close to the following extension

$$g = \sum_{j=1}^2 g_j \Omega_j, \quad h = \sum_{j=1}^2 h_j \Omega_j \quad \text{and} \quad \theta = \sum_{j=1}^2 \theta_j \Omega_j, \quad (30)$$

where f_j, h_j and θ_j as Ω_j are linear shape functions and uncharted nodal values. Used in upper nodal similarity by the field variables on powerless formation of weighted fragment, once access the sketch over finite element on the pattern

$$[K^e \{\pi\}][\pi^e] = \{Q^e\} + \{F^e\}, \quad (31)$$

here, $[\pi^e]$ was unknown nodal values, $[K^e \{\pi\}]$ is stiffness matrix of typical component, $\{Q^e\}$ as the source vector and $\{F^e\}$ as the boundary vector. The boundary elements and stiffness were taken as

$$K_{ij}^{11} = \int_{\xi_b}^{\xi_{b+1}} \Omega_i \frac{d\Omega_j}{d\xi} d\xi, \quad K_{ij}^{12} = - \int_{\xi_b}^{\xi_{b+1}} \Omega_i \Omega_j d\xi, \quad K_{ij}^{13} = 0, \quad (32)$$

$$\begin{aligned} K_{ij}^{22} = & - \left(\frac{1}{\varphi_a \varphi_b} + \frac{\omega}{\varphi_a} - \frac{\omega \Delta}{\varphi_b h^2} \right) \int_{\xi_b}^{\xi_{b+1}} \frac{d\Omega_i}{d\xi} \frac{d\Omega_j}{d\xi} d\xi \\ & + \bar{g} \int_{\xi_b}^{\xi_{b+1}} \Omega_i \frac{d\Omega_j}{d\xi} d\xi - \bar{h} \int_{\xi_b}^{\xi_{b+1}} \Omega_i \Omega_j d\xi - A \int_{\xi_b}^{\xi_{b+1}} \Omega_i \Omega_j d\xi \\ & - A \frac{\xi}{2} \int_{\xi_b}^{\xi_{b+1}} \Omega_i \frac{d\Omega_j}{d\xi} d\xi, \quad K_{ij}^{21} = K_{ij}^{23} = 0, \end{aligned} \quad (33)$$

$$\int_{\xi_{b+1}}^{\xi_b} w_i \left(\frac{1}{\varphi_c} \left(1 + \frac{4Rd}{3\varphi_d} (1 + (\theta_w - 1)\theta)^3 \right) \theta'' + \frac{4}{\varphi_c \varphi_d} Rd (1 + (\theta_w - 1)\theta)^2 (\theta_w - 1)\theta'^2 + \Pr \frac{\varphi_c}{\varphi_d} \left[g \theta' - h\theta - A \left(\theta + \frac{\xi}{2} \theta' \right) + \frac{Ec}{\varphi_a \varphi_c} h^2 + \frac{Q}{\varphi_c} \theta e^{-\xi} \right] \right) d\xi = 0, \quad (29)$$

where $g' = h$ and $w_i (i = 1, 2)$ was weight functions into reduce the fragment identical for f, θ and h . This uncharted

$$\begin{aligned}
 K_{ij}^{33} = & -\frac{1}{\varphi_c} \left(1 + \frac{4\text{Rd}}{3\varphi_d} (1 + (\theta_w - 1)\bar{\theta})^3 \right) \int_{\xi_b}^{\xi_{b+1}} \frac{d\Omega_i}{d\xi} \frac{d\Omega_j}{d\xi} d\xi \\
 & + \frac{4}{\varphi_c \varphi_d} \text{Rd} (1 + (\theta_w - 1)\bar{\theta})^2 (\theta_w - 1) \bar{\theta}' \int_{\xi_b}^{\xi_{b+1}} \Omega_i \frac{d\Omega_j}{d\xi} d\xi \\
 & + \text{Pr} \frac{\varphi_c}{\varphi_d} \bar{g} \int_{\xi_b}^{\xi_{b+1}} \Omega_i \frac{d\Omega_j}{d\xi} d\xi - \text{Pr} \frac{\varphi_c}{\varphi_d} \int_{\xi_b}^{\xi_{b+1}} \Omega_i \Omega_j d\xi \\
 & - \text{Pr} \frac{\varphi_c}{\varphi_d} A \int_{\xi_b}^{\xi_{b+1}} \Omega_i \Omega_j d\xi \\
 & - \text{Pr} \frac{\varphi_c}{\varphi_d} A \frac{\xi}{2} \int_{\xi_b}^{\xi_{b+1}} \Omega_i \frac{d\Omega_j}{d\xi} d\xi + \text{Pr} \frac{Q}{\varphi_d} e^{-\xi} \int_{\xi_b}^{\xi_{b+1}} \Omega_i \Omega_j d\xi, \\
 K_{ij}^{32} = & \text{Pr} \frac{\text{Ec}}{\varphi_d \varphi_a} \bar{h}' \int_{\xi_b}^{\xi_{b+1}} \Omega_i \frac{d\Omega_j}{d\xi} d\xi, \quad K_{ij}^{31} = 0,
 \end{aligned} \tag{34}$$

and

$$\begin{aligned}
 b_{ij}^1 = 0, \quad b_{ij}^2 = & -\left(\frac{1}{\varphi_a \varphi_b} + \frac{\omega}{\varphi_a} - \frac{\omega \Delta}{\varphi_b} \bar{h}^{-2} \right) \int_{\Gamma} \Omega_i \frac{d\Omega_j}{d\xi} d\Gamma, \\
 b_{ij}^3 = & -\frac{1}{\varphi_c} \left(1 + \frac{4\text{Rd}}{3\varphi_d} (1 + (\theta_w - 1)\bar{\theta})^3 \right) \int_{\Gamma} \Omega_i \frac{d\Omega_j}{d\xi} d\Gamma.
 \end{aligned} \tag{35}$$

$$\begin{aligned}
 \text{Subsequently where } \bar{g} = \sum_{j=1}^2 \bar{g}_j \Omega_j, \quad \bar{h} = \sum_{j=1}^2 \bar{h}_j \Omega_j \text{ and } \bar{\theta} \\
 = \sum_{j=1}^2 \bar{\theta}_j \Omega_j.
 \end{aligned} \tag{36}$$

4.5. Assembly process

The Elemental connectedness was worked about assembly method. To accepting the upper similarity into every component, once again that system of nonlinear algebraic equations on the pattern

$$[K\{\pi\}][\pi] = \{Q\} + \{F\}. \tag{37}$$

Insistent process was unfamiliar into clarify the system of equations. That structure was linearized as Picard's linearization method. This system of algebraic equations was defined numerically to utilize Gauss–Seidel path.

4.6. Error analysis and convergence

These faults were coordinated as applying

$$\text{Error} = |\pi^r - \pi^{r-1}| \tag{38}$$

And conduct about the confluence was determined by $\max |\pi_i^r - \pi_i^{r-1}| < 10^{-5}$.

4.7. Validation of results

Acceptance of numerical program was gained as connection about heat transport rate by the boundary. Outcomes determined over current code are related into outcomes announced as [3, 29, 30] and are sequential in Table 2. Ref. [3] studied the entropy generation of Powell–Eyring hybrid nanofluid. Ref. [29] discussed the analysis of entropy for unsteady flow over a permeable surface. Ref. [30] analyzed the unsteady magneto-nanofluid flow over accelerating surface. An excellent compliance is recognized in Table 2, among outcome gained against the current program and these particular applicable on the literature.

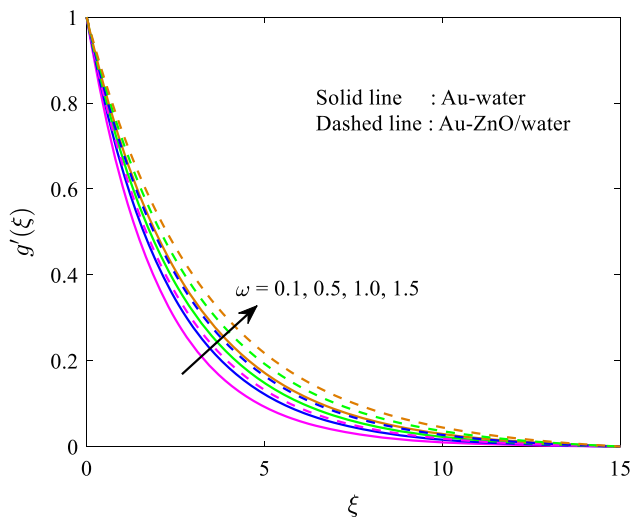
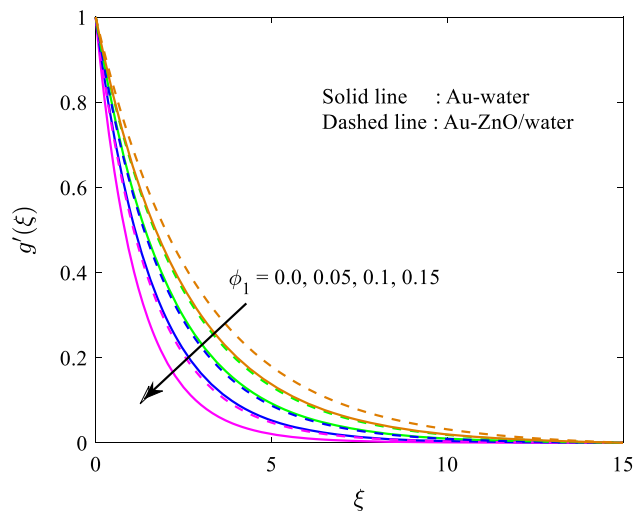
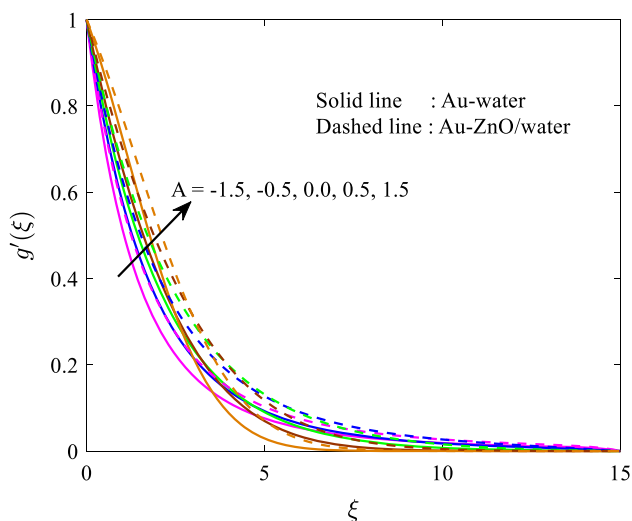
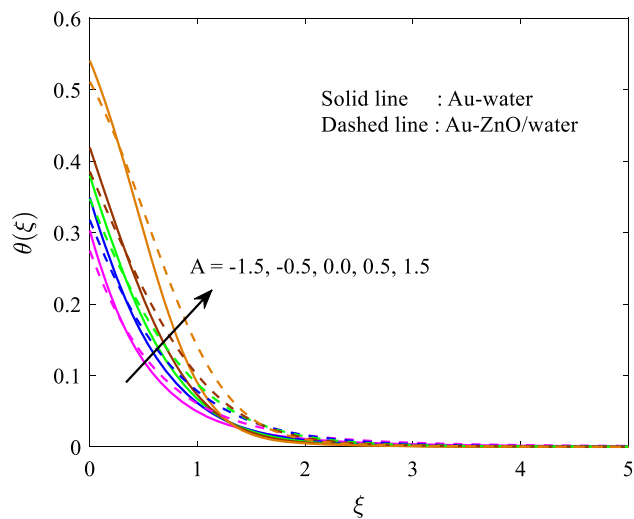
5. Results and discussion

In that area, calculation imposed analysis impact on material parameter ω , nanoparticle volume concentration parameters φ_1 , Eckert number Ec, radiation parameter Rd, heat source/sink parameter Q , Brinkman number Br on fluid motion, local Reynolds number Re Biot number Bi and the all volumetric entropy generation to humanistic and hybrid nanofluid and temperature variation. Outcomes were descriptive in Figs. 2, 3, 4, 5, 6, 7, 8, 9, 10, 11 and 12. Further, Table 3 extracts impact on governing parameters in temperature gradient in the boundary. Calculation was borne because both Au–H₂O conventional nanofluid and (Au–ZnO/H₂O) hybrid nanofluid. To reveal the parametric effect, we have assigned the parametric values as Pr = 6.2, $\omega = 0.5$, $\Delta = 0.2$, Rd = 0.2, $A = 0.1$, $\varphi_1 = 0.1$, $Q = 0.1$, $\theta_w = 2.0$, $\varphi_2 = 0.1$, Bi = 1.2, Ec = 0.1 unless otherwise mentioned. The range of parameters such that $0.1 \leq \omega \leq 1.5$, $0.0 \leq A \leq 1.5$, $0.0 \leq \varphi_1 \leq 0.15$, $0.6 \leq \text{Rd} \leq 1.2$, $0.0 \leq \text{Ec} \leq 0.6$, $-0.8 \leq Q \leq 0.8$, $0.3 \leq \text{Bi} \leq 0.6$, $0.1 \leq \text{Br} \leq 1.0$, $4.0 \leq \Omega \leq 16$, $0.4 \leq \text{Re} \leq 0.7$.

Figure 2 presents impact on material fluid parameter ω in velocity distribution for the Powell–Eyring hybrid nanofluid and the Powell–Eyring nanofluid, appropriately. Calculation was performed being $\omega = 0.1, 0.5, 1.0, 1.5$ at nanoparticles volume friction of $\phi_1 = 0.1$ and $\phi_2 = 0.1$. Ascending direction on velocity profiles was noticed about developing values on ω , and that raised the density away from momentum boundary layer. Therefore, ω was inversely proportional to the base fluid viscosity, expansion on definite values of ω reduces enlarge the stress rate and the base fluid viscosity inside the boundary layer. Decision to that velocity away from hybrid and convectional rises

Table 2 Correlation of $-\theta'(0)$ into variation on Pr, and giving $A = 0$, $\omega = 0$, $Rd = 0$, $Q = 0$ and $Bi = 0$

Pr	Abolbashari results [29]	Das results [30]	Aziz et al. [3]	Present
0.72	0.80863135	0.80876122	0.80876181	0.80863711
1.0	1.00000000	1.00000000	1.00000000	1.00000006
3.0	1.92368259	1.92357431	1.92357420	1.92368257
7.0	3.07225021	3.07314679	3.07314651	3.07225019
10.0	3.72067390	3.72055436	3.72055429	3.72067388

**Fig. 2** Velocity $g'(\xi)$ against ω **Fig. 4** Velocity $g'(\xi)$ against ϕ_1 **Fig. 3** Velocity $g'(\xi)$ against A **Fig. 5** Temperature $\theta(\xi)$ against A

inside boundary layer. This impact on ω in the viscosity on base fluid could be seen over change on skin friction factor of Fig. 11. The skin friction factor for the boundary believes increasing direction. Further, being stable value of ω , that density of momentum boundary layer about hybrid

nanofluid was extra during related into the classical nanofluid. The results in Fig. 11 show that the hybrid nanofluid (Au-ZnO/water) has less skin friction than the nanofluid (Au-water).

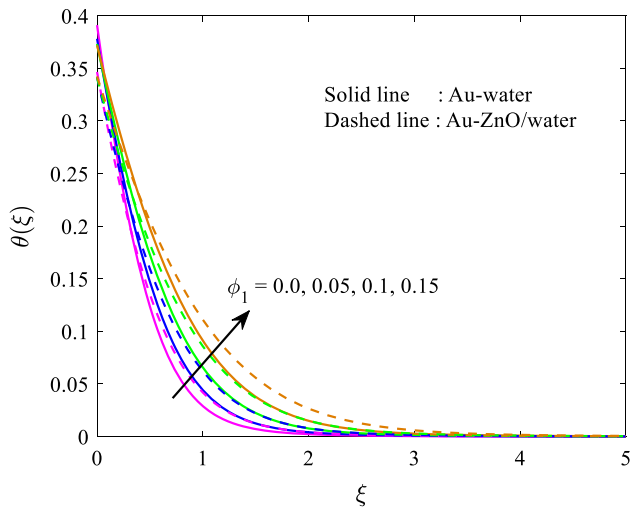


Fig. 6 Temperature $\theta(\xi)$ against ϕ_1

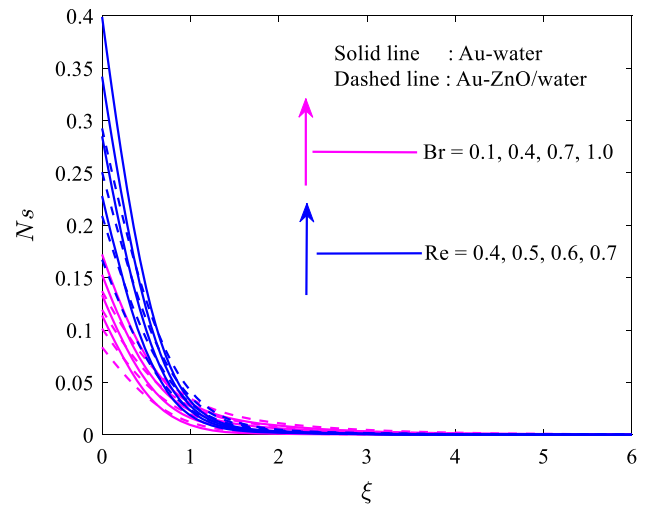


Fig. 9 Entropy N_s against Re and Br

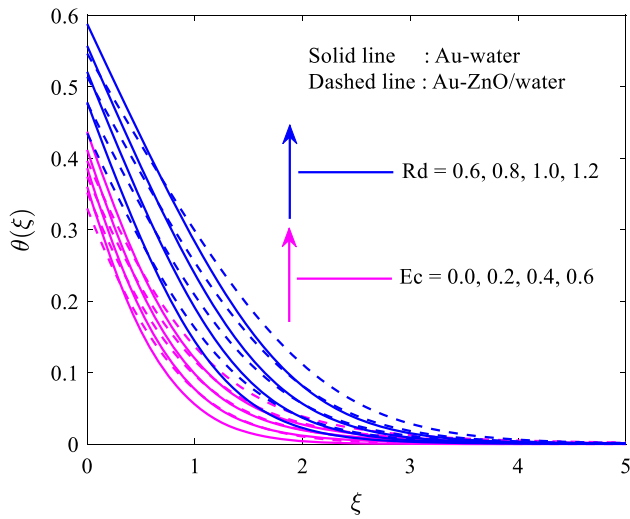


Fig. 7 Temperature $\theta(\xi)$ against Rd and Ec

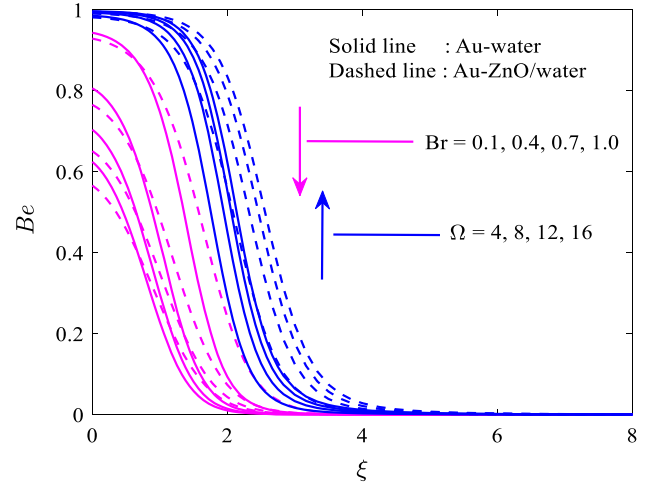


Fig. 10 Bejan number Be against Ω and Br

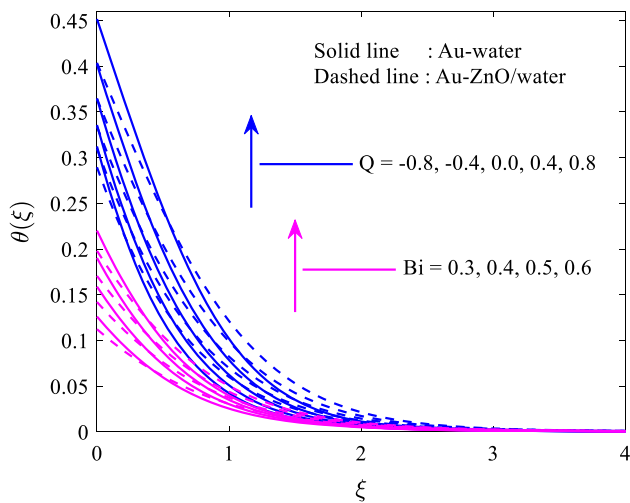


Fig. 8 Temperature $\theta(\xi)$ against Q and Bi

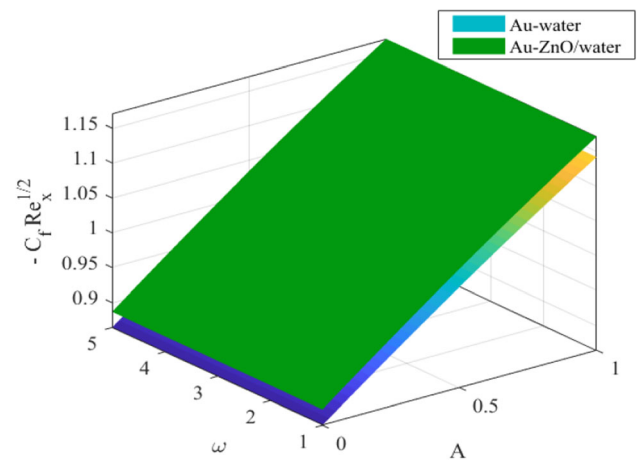


Fig. 11 Skin friction $C_f Re_x^{1/2}$ against ω and A

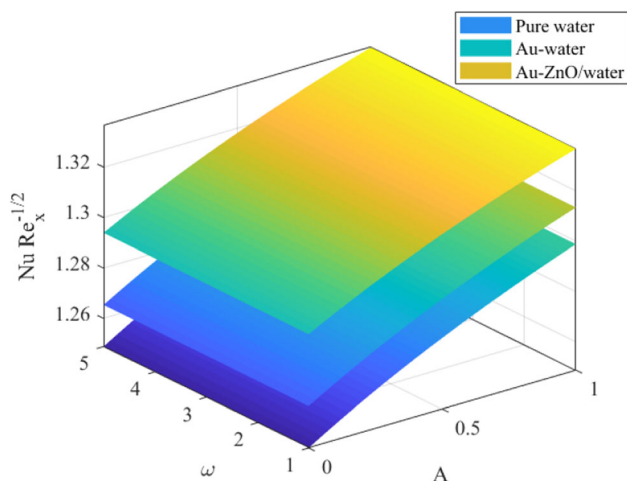


Fig. 12 Nusselt number $Nu Re_x^{-1/2}$ against ω and A

The variation in $g'(\xi)$ is illustrated in Fig. 3 versus the change on unsteady parameter A for both usual nanofluid and hybrid nanofluid. Here, $A = 0$ conform to steady-state flow problem, $A > 0$ perform quick flow on that case alone devoted flow solution was generated, during $A < 0$ display decelerated flow; on that case, two characters of results are gained contained by obsessed flow solution and opposite flow solution. Figure 3 displays this increasing the value of A raises the velocity to the fluid. That fundamental physics after that direction was as long as of the reducing pressure in the trend of flow as the increase on A that margin to embellished velocity of the fluid. That outcomes were dependent into these gained as Mabood et al. [13] and Sadiq et al. [24]. Furthermore, it was noticed against the plot to the strength of Au-ZnO hybrid nanofluid was grater rapid when related to the usual nanofluid.

Effect of Au nanoparticle volume friction parameters ϕ_1 on velocity distribution is presented in Fig. 4. In Fig. 4, velocity about Au as lesser outstanding the fact that Au nanofluid profile greater density effect into the gain on ϕ_1 by related to hybrid nanofluid. Previous investigations [3, 13] also reported the same observation. The variation in temperature distribution is illustrated in Fig. 5 from the alteration on unsteady parameter A . At present, they study the certain cases $A = -1.5, -1, 0, 1, 1.5$ impartial to analyze by demeanor on boundary layer flow about the unsteady state and steady state. It saw the accelerating values of A addition the thermal distributions of the fluid. That outcome came through into that gained as Sadiq et al. [24] and Mabood et al. [13]. Further, an enhanced temperature is perfect about hybrid nanofluid outstanding the existence of dual slight mixtures than the usual nanofluid.

Figure 6 displays growth on fluid the contraction and temperature on heat transfer rate among developing values of nanoparticles concentration on this base fluid. This was

expected greater thermal conductivity by solid particles whatever increment that total thermal conductivity on nanofluid. Furthermore, the destruction with nanoparticles consumes heat energy on the system and development the total temperature. They were anticipating to that temperature on hybrid nanofluid advance by the rapid rate due to related into conventional nanofluids.

That was no impact on Eckert number Ec , Biot number Bi and, thermal radiation parameter Rd on the velocity profiles. Rises on thermal radiation measure higher heat were coming with the temperature and system to nanofluid increases outstanding that. Figure 7 certifies that case and increase on radiation parameter Rd improve the nanofluid temperature inside boundary layer. Substantially speaking that strengthening on parameter Rd alteration extra heat with a fluid and increase the thermal boundary layer density for both traditional nanofluid Au-H₂O and hybrid nanofluid ZnO-Au/H₂O. The Eckert number Ec as ratio on the kinetic energy of the enthalpy (or the dynamic temperature into the temperature), and the higher values of Ec involve higher kinetic energy about nanoparticles these performance by the driving force about greater rate of heat transfer. Every frictional heating given to the surface allowing growth for the temperature to the comparable nanofluid (seen Fig. 7).

Every graph on temperature profile $\theta(\xi)$ about the excessive values of thermal Biot number (Bi) and aggressive heat source parameter Q is displayed in Fig. 8. It explains the temperature field enhance about raise values of Q and Bi . Physically, $Q > 0$ measure high heat would be activated against the surface on the fluid. So, temperature sketch grows about the development Q values. Moreover, Bi raises transfer to heat over convection given place broadly. Thus, increase in temperature field could be seen. It was worth observing that effect of parametric values closed hybrid nanofluid was extremely affected when related into mono-nanofluid.

The impact on Brinkman number Br and Reynolds number Re in the overall volumetric entropy generation rate is granted in Fig. 9. Greater value of Re increases the total entropy. That produces the dominance on inertial forces by the viscous forces. Overly, by enlargement on Brinkman number Br raises the entropy generation rate. The same was reported by Aziz et al. [3]. They current the effect on pertinent parameters in the Bejan number is shown in Fig. 10. It reduces in Bejan number by parameter Br proved this heat transfer irreversibility effect dominates to fluid friction effects. The opposite performance was observed by developing values on Ω . Furthermore, the impacts on hybrid nanoparticles are higher than formal nanoparticles.

Figures 11 and 12 build the alteration on Nusselt number and skin friction coefficient by the three fluids, namely

Table 3 Numerical values of Nusselt number about different parametric values are $Pr = 6.2$, $A = 0.1$ and $\omega = 0.5$

Rd	Q	Ec	θ_w	Bi	NuRe _x ^{-1/2}		
					Pure water	Au-water	Au–ZnO/water
0.0	0.1	0.1	2.0	1.2	0.814414	0.823761	0.848495
0.2					1.255174	1.271484	1.299365
0.4					1.732456	1.751605	1.781079
0.6					2.219459	2.243896	2.280824
Sp					2.346209	2.370263	2.389351
0.2	– 0.4				1.292385	1.303703	1.324699
					1.279287	1.292229	1.315545
	– 0.2	0.0			1.263914	1.278947	1.305131
		0.2			1.245594	1.263376	1.293167
	0.4			1.223369	1.244850	1.279262	
	Sp				– 11.5201	– 13.5247	– 17.5398
	0.0				1.279442	1.282945	1.308583
	0.2				1.229806	1.259749	1.289952
	0.4				1.175560	1.235419	1.270511
	0.6				1.116345	1.209886	1.250206
	Sp				– 0.27177	– 0.12175	– 0.09729
	1.5				1.098550	1.119905	1.155937
	2.5				1.496443	1.503008	1.513353
3.5				2.466739	2.464557	2.422600	
4.5				4.331971	4.305796	4.345728	
Sp				1.067056	1.051922	1.047862	
				0.1	0.123117	0.124046	0.124377
				0.3	0.359102	0.362001	0.364046
				0.5	0.581751	0.586932	0.592090
				0.7	0.791049	0.798925	0.808673
				Sp	1.113223	1.124784	1.140466

regular nanofluid, base fluid and hybrid nanofluid. In Figs. 12 and 13, it was observed this Nusselt number and skin friction coefficient was rising as development material parameter (ω) and unsteadiness parameter (A). Furthermore, the improved heat transfer rate was entire hybrid nanofluid when the occupation on dual slight mixtures of the usual nanofluid. By exposed against the equal plot, lessor heat was transmitted as pure base fluid ($\phi_1 = \phi_2 = 0$).

The nature of variation in Nusselt number when the various parameters are computed in Table 3 utilizes the slope of linear regression about the three fluids, namely base fluid, hybrid nanofluid and regular nanofluid. The positive slope implicit to the corresponding parameter improves the heat transfer rate. The magnitude on slope performs the rate of raises/reduce on Nusselt number through unit value on the corresponding parameters.

Utilizing the slope by linear relapse through the information points, they were depicted to the numerical values

by the Nusselt number (heat transfer rate) raises gradually into radiation parameter (Rd at the rates 2.346209, 2.370263 and 2.389351, respectively, for the pure water, Au-water and ZnO–Au/water. However, heat source/sink parameter (Q) reduces the Nusselt number at the rates –11.5201, –13.5247 and –17.5398 correspondingly for base fluid, nanofluid and hybrid nanofluid. To local Nusselt number (Nu) increases at the rates 1.067056, 1.051922 and 1.047862 for θ_w , respectively, for pure water, nanofluid and hybrid nanofluid. The heat transfer rate increases as the rate of 1.113223, 1.124784 and 1.140466 via Biot number (Bi) for base fluid, Au-water and Au-ZnO/water; however, the Nu decreases at the rate of –0.27177, –0.12175 and –0.09729 via Eckert number (Ec), respectively, for pure water, nanofluid and hybrid nanofluid. Finally, the Au–ZnO/water hybrid nanoliquid has greater heat transfer rate to that regular fluid (pure water) and nanofluid (Au–water).

6. Conclusions

The present article concentrates mainly to heat transfer and entropy generation when the fluid flow on Powell–Eyring hybrid nanofluid considering aggressive space-dependent heat source and nonlinear thermal radiation into convective heat flux boundary condition. That nanofluid employs field over the infinite absorbent stretching surface. Numerical calculations were transported about pure water ($\phi_1 = \phi_2 = 0$), gold water (Au–H₂O) nanofluid and zinc oxide–gold water (ZnO–Au/H₂O) hybrid nanofluids. The equations of the stated flow are defined numerically by finite element method, and graphs were plotted utilizing gained numerical values. They had related the current analysis outcomes into the existing solutions, and that was on par into the earlier outcomes. The following conclusions could be made about their analysis: An increment on concentration of nanoparticles, the velocity profile reduces and raising direction had been noticed as temperature profile. Improvement on unsteadiness parameter raises every temperature and velocity profiles. Both Eckert number and Biot number had the developing effect on temperature field. The Powell–Eyring hybrid nanofluid (ZnO–Au/H₂O) was noticed to be the best thermal conductor than the pure fluid ($\phi_1 = \phi_2 = 0$) and conventional Powell–Eyring nanofluid (Au–H₂O). Total entropy of the system was noticed to rise into develop on Brinkman number and Reynolds number. The Nusselt number is highly positive impact with the radiation parameter and Biot number, and highly negative impact with heat source parameter and Eckert number using the linear regression model. Bejan number is increasing function for Brinkman number and decreasing function of Ω .

That analysis could supply the best understanding to other investigators to the topic on hybrid nanofluids especially on that convective heat flux condition. It was important to that the best heat transfer achievement on more technological and industrial method. By the future works, it was proposed to the current analysis that will be consummate into more nanoparticles (metallic or non-metallic) along into different base fluids (like diathermic oil or SAE oil). That was crucial about the collection to optimum hybrid nanofluid into accomplish the minimum skin friction and maximum heat transfer rate by heat transfer functions.

Declarations

Conflict of interest The authors declare that there is no conflict of interest.

References

- [1] R Powell and H Eyring *Nature* **154** 427 (1944)
- [2] M Patel and M G Timol *Appl. Numer. Math.* **59** 84 (2009)
- [3] A Aziz, W Jamshed, T Aziz, H M S Bahaidarah and L U Khalil Ur Rehman *J. Therm. Anal. Calorim.* **143** 1331 (2021)
- [4] K Vafai, A A Khan, G Fatima, S M Sait and R Ellahi *Int. J. Numer. Methods Heat Fluid Flow* **31** 1085 (2021)
- [5] W F Xia, F Haq, M Saleem, M Ijaz Khan, S U Khan and Y M Chu *Ain Shams Eng. J.* **12** 4063 (2021)
- [6] M G Ibrahim *Int. Commun. Heat Mass Transf.* **134** 105987 (2022)
- [7] S U S Choi *Conference: 1995 international mechanical engineering congress and exhibition, San Francisco, CA*, p 12 (1995)
- [8] G Lu (Berlin: Springer) (2016)
- [9] K Gangadhar, D Vijaya Kumar, M Venkata Subba Rao, T Kannan and G Sakthivel *Int. J. Ambient Energy* **43** 1248 (2022)
- [10] J Lee, S Lee, C Cho and S Kim *Int. J. Heat Mass Transf.* **192** 122941 (2022)
- [11] J Sarkar, P Ghosh and A Adil *Renew. Sust. Energ. Rev.* **43** 164 (2015)
- [12] J R Babu, K K Kumar and S S Rao *Renew. Sust. Energ. Rev.* **77** 551 (2017)
- [13] F Mabood, G P Ashwinkumar and N Sandeep *J. Therm. Anal. Calorim.* **146** 227 (2021)
- [14] F Selimefendigil and H F Oztop *Int. J. Heat Mass Transf.* **178** 121623 (2021)
- [15] N Abbas, K U Rehman, W Shatanawi and M Y Malik *Int. Commun. Heat Mass Transf.* **135** 106107 (2022)
- [16] W Cao, L Animasaunl, S J Yook, V A Oladipupo and X Ji *Int. Commun. Heat Mass Transf.* **135** 106069 (2022)
- [17] Y Zhai, P Yao, X Shen and H Wang *Int. Commun. Heat Mass Transf.* **135** 106118 (2022)
- [18] J M Avellaneda, F Bataille, A Toutant and G Flamant *Int. J. Heat Mass Transf.* **176** 121463 (2021)
- [19] N R Devi, S Moolya, H F Oztop, N Abu-Hamdeh, P Padmanathan and A Satheesh *Eur. Phys. J. Plus* **137** 482 (2022)
- [20] S Gowtham, C Sivaraj and M A Sheremet *Eur. Phys. J. Plus* **137** 510 (2022)
- [21] S Marzougui, F Mebarek-Oudina, M Magherbi and A Mchirgui *Int. J. Numer. Methods Heat Fluid Flow* **32** 2047 (2022)
- [22] Z Sarbazi and F Hormozi *Int. J. Numer. Methods Heat Fluid Flow* **32** 62 (2022)
- [23] S K Mehta, S Pati, S Ahmed, P Bhattacharyya and J J Bordoloi *Int. J. Numer. Methods Heat Fluid Flow* **32** 1618 (2022)
- [24] M N Sadiq, B Sarwar, M Sajid and N Ali *J. Therm. Anal. Calorim.* **147** 5199 (2022)
- [25] B Nagaraja, B J Gireesha and J Therm Anal. Calorim. **143** 4071 (2021)
- [26] H Berrehal, G Sowmya and O D Makinde *Int. J. Numer. Methods Heat Fluid Flow* **32** 1643 (2022)
- [27] W M Qian, M Ijaz Khan, F Shah, M Khan, Y M Chu, W A Khan and M Nazeer *Arab. J. Sci. Eng.* **47** 867 (2022)
- [28] K Gangadhar, D Naga Bhargavi, M Venkata Subba Rao and A J Chamkha *Phys. Scr.* **96** 095205 (2021)
- [29] M H Abolbashari, N Freidoonimehr, F Nazari and M M Rashidi *Powder Technol.* **267** 256 (2014)
- [30] S Das, S Chakraborty, R N Jana and O D Makinde *Appl. Math. Mech.* **36** 1593 (2015)
- [31] S Dinarvand and I Pop *Adv. Powder Technol.* **28** 900 (2017)
- [32] M Aghamajidi, M Eftekhari Yazdi, S Dinarvand and I Pop *Propuls. Power Res.* **7** 78 (2018)
- [33] H A Mohammed, A N Al-Shamani and J M Sheriff *Int. Commun. Heat Mass Transf.* **39** 1584 (2012)

- [34] R S Vajjha and D K Das *Int. J. Heat Mass Transf.* **52** 4675 (2009)
- [35] D Srinivasacharya, U Mendu and K Venumadhav *Procedia Eng.* **127** 1064 (2015)
- [36] S Wang, B Zeng and C Li *Chin. J. Catal.* **39** 1219 (2018)
- [37] R J Tiwari and M K Das *Int. J. Heat Mass Transf.* **50** 2002 (2007)
- [38] W Jamshed and A Aziz *Results Phys.* **9** 195 (2018)
- [39] E Magyari and A Pantokratoras *Int. Commun. Heat Mass Transf.* **38** 554 (2011)
- [40] P Kumam, Z Shah, A Dawar, H Ur-Rasheed and S Islam *Math. Probl. Eng.* **2019** 1 (2019)
- [41] T Tayebi, A J Chamkha, A A Melaibari and E Raouache *Int. Commun. Heat Mass Transf.* **126** 105397 (2021)
- [42] S A M Mehryan and M Ghalambaz *J. Energy Storage* **28** 101236 (2020)
- [43] M Ghalambaz, S A M Mehryan, A Hajjar and A Veismoradi *Adv. Powder Technol.* **31** 3 954 (2020)
- [44] M Ghalambaz, T Grosan and I Pop *J. Mol. Liq.* **293** 111432 (2019)
- [45] M S Sadeghi et al. *J. Therm. Anal. Calorim.* **147** 1 (2022)
- [46] M A Mansour, T Armaghani, A J Chamkha and A M Rashad *Eur. Phys. J. Spec. Top.* **228** 2619 (2019)
- [47] S Hussain, T Armaghani and M Jamal *J. Thermophys. Heat Trans.* **34** 203 (2020)
- [48] K Ayoubi Ayoubloo, M Ghalambaz, T Armaghani, A Noghrehabadi and A J Chamkha *Int. J. Numer. Methods Heat Fluid Flow* **30** 1096 (2020)
- [49] A I Alsabery, T Armaghani, A J Chamkha, M A Sadiq and I Hashim *Int. J. Numer. Methods Heat Fluid Flow* **29** 1272 (2019)

Publisher’s Note Springer Nature remains neutral with regard to jurisdictional claims in published maps and institutional affiliations.

Springer Nature or its licensor (e.g. a society or other partner) holds exclusive rights to this article under a publishing agreement with the author(s) or other rightsholder(s); author self-archiving of the accepted manuscript version of this article is solely governed by the terms of such publishing agreement and applicable law.